A multi-analytical approach to stream-sediment samples from modern drainages enhances the search for REE and rare metals

Alexei S. Rukhlov[1, a], Luke Ootes[1], Quinn F. Cunningham[1], Dylan Goudie[2], Anette von der Handt[3], Jody Spence[4], Corey Wall[5], and Shaun Barker[6]

[1] British Columbia Geological Survey, Ministry of Mining and Critical Minerals, Victoria, BC, V8W 9N3
[2] Core Research Equipment and Instrument Training (CREAIT) Network, Memorial University of Newfoundland, 45 Arctic Avenue, St. John's, NL, A1C 5S7
[3] Electron Microbeam & X-Ray Diffraction Facility, Department of Earth, Ocean and Atmospheric Sciences, The University of British Columbia, Vancouver, BC, V6T 2B4
[4] School of Earth and Ocean Sciences, University of Victoria, Victoria, BC, V8P 5C2
[5] Pacific Centre for Isotopic and Geochemical Research, Department of Earth, Ocean and Atmospheric Sciences, The University of British Columbia, Vancouver, BC, V6T 1Z4
[6] Mineral Deposits Research Unit, Department of Earth, Ocean and Atmospheric Sciences, The University of British Columbia, Vancouver, BC, V6T 2B4
[a] corresponding author: Alexei.Rukhlov@gov.bc.ca

Recommended citation: Rukhlov, A.S., Ootes, L., Cunningham, Q.F., Goudie, D., von der Handt, A., Spence, J., Wall, C., and Barker, S., 2026. A multi-analytical approach to stream-sediment samples from modern drainages enhances the search for REE and rare metals. In: Geological Fieldwork 2025, British Columbia Ministry of Mining and Critical Minerals, British Columbia Geological Survey Paper 2026-01, pp. 97-117.

Abstract

Mineralogical assessment of stream-sediment samples downstream of known carbonatite and related-rock occurrences confirms the occurrence of such rocks in the catchment basin upstream. Application of qualitative X-ray diffraction, quantitative evaluation of minerals by scanning electron microscopy (QEMSCAN®), scanning electron microscopy-mineral liberation analysis (SEM-MLA) and micro-X-ray fluorescence (μXRF) identify minerals such as columbite, pyrochlore supergroup, other Nb-Ta oxides, and REE carbonate contained in stream sediments. Chemistry of detrital minerals such as zircon and apatite and application of discrimination diagrams are further indicators of enhanced prospectivity of the drainages. These preliminary results suggest that micro-analysis (SEM-MLA, μXRF) on stream-sediment samples, in conjunction with detrital mineral chemistry, can enhance the interpretation of multivariate Regional Geochemical Survey (RGS) lithogeochemical anomalies of modern drainages and help identify prospective catchment basins for REE, Nb, Ta, and other commodities. The indicator-mineral approach applied to archived RGS samples informs prospectivity for critical minerals at a regional scale.

Keywords: Scanning electron microscopy-mineral liberation analysis (SEM-MLA), carbonatite, alkaline rock, stream sediment, heavy mineral concentrate (HMC), rare metals, rare earth elements (REE), zircon, apatite

1. Introduction

Niobium and rare earth elements (REE) are mainly produced from carbonatites and related silica-undersaturated and alkaline silicate rocks. British Columbia hosts numerous occurrences of these rocks along the western flank of Ancestral North America (Fig. 1), some of which contain REE and Nb-Ta mineralization (e.g., Mäder, 1987; Pell, 1994; Dalsin et al., 2015; Kulla and Hardy, 2015; Rukhlov et al., 2018). Based on Regional Geochemical Survey (RGS) data and machine learning, Rukhlov et al. (2024) evaluated the prospectivity of modern drainage catchments in terms of a multivariate critical mineral index. Samples with high scores of this index have a lithogeochemical response that suggests the occurrence of carbonatite- or related rock-hosted rare metals and REE in the catchment basin upstream.

This study continues the drainage prospectivity assessment (Rukhlov et al., 2025a). We consider previously reported lithogeochemical and new grain count data from two of our nine sampling sites (downstream of the Switch Creek and Ren (Ratchford Creek) carbonatites; Fig. 1) and provide new data from qualitative X-ray diffraction analysis, quantitative evaluation of minerals by scanning electron microscopy (QEMSCAN®), scanning electron microscopy-mineral liberation analysis (SEM-MLA), micro-X-ray fluorescence (μXRF), detrital zircon and apatite trace-element analysis, and U-Pb detrital zircon geochronology. Indicator minerals identified confirm the occurrence of carbonatites in the catchment basins upstream.

2. Sampling

We collected a total of 36 stream-sediment samples from nine drainage sites downstream of carbonatite and related-rock occurrences, or related RGS anomalies (Fig. 1; Table 1). To inform the optimal medium, we examined both panned,

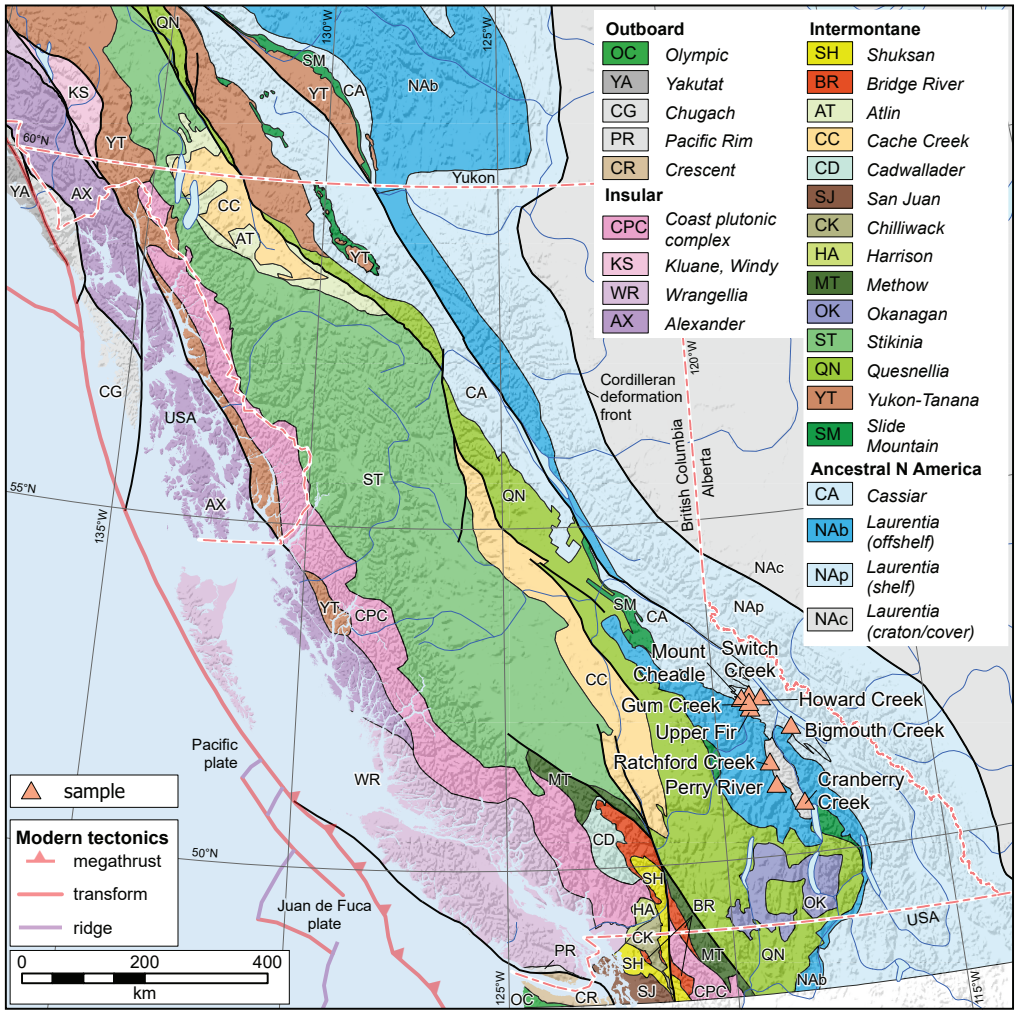

Fig. 1. Sampling sites, southeastern British Columbia. Terranes modified from Colpron (2020).

heavy-mineral concentrate (HMC) and bulk stream-sediment samples, both fine (<0.18 mm) and coarse (0.18-1.0 mm) fractions. Below we focus on samples collected downstream of the Switch Creek (Fig. 2) and Ren (Ratchford Creek; Fig. 3) carbonatites.

3. Qualitative X-ray diffraction analysis

A representative portion of each sample was split using micro-riffle splitter at Activation Laboratories Ltd. (Ancaster, Ontario). A qualitative X-ray diffraction analysis was performed on a Bruker D8 Endeavour diffractometer equipped with Cu X-ray source and operating at the following conditions: 40 kV and 40 mA; range 4-70° 2Θ; step size 0.02° 2Θ; time per step 0.5 seconds; fixed divergence slit, angle 0.30°; sample rotation 15 rpm. The PDF4/Minerals ICDD database was used for mineral identification. Minerals that were identified include: quartz, plagioclase, K-feldspar, Ca-Na amphibole, diopside/augite, almandine, kyanite, muscovite, biotite, chlorite, smectite, apatite, magnetite, and dolomite.

4. Scanning electron microscopy

4.1. Quantitative evaluation of minerals by scanning electron microscopy (QEMSCAN®)

Quantitative mineralogical analysis was carried out using a FEI QEMSCAN® field emission gun scanning electron microscope (SEM) at Activation Laboratories Ltd. (Ancaster, Ontario). Approximately 2 g of material was embedded in epoxy resin for preparing round polished grain mounts (30 mm diameter). Two grain mounts were made per sample: normal and transverse (cross-section). Transverse sections were used for bulk modal mineralogy and normal sections for trace mineral search. Minerals are identified using energy dispersive X-ray spectroscopy (EDS) spectra, which are indicative of mineral chemistry. Therefore, minerals with similar chemical composition (e.g., kyanite and sillimanite) cannot be resolved. Additionally, elements with atomic number (Z) of <11 (Na) cannot be detected. Particles <10 µm (i.e., close to the beam spot spacing) may not be detected.

Table 1. Stream-sediment samples. For full details see Rukhlov et al. (2025b).

Id	Site Id	Locality	Latitude	Longitude	Fraction
1	24ARU-2001	Bigmouth Creek	51.904038	-118.222807	<0.18 mm; BSS
2					0.18 to 1.0 mm; BSS
3					<0.18 mm; HMC
4					0.18 to 1.0 mm; HMC
5	24ARU-2002	Switch Creek	52.413113	-119.149492	<0.18 mm; BSS
6					0.18 to 1.0 mm; BSS
7					<0.18 mm; HMC
8					0.18 to 1.0 mm; HMC
9	24ARU-2003a	Howard Creek	52.363868	-118.868337	<0.18 mm; BSS
10					0.18 to 1.0 mm; BSS
11					<0.18 mm; HMC
12					0.18 to 1.0 mm; HMC
13	24ARU-2003b	Mount Cheadle	52.326285	-119.164279	<0.18 mm; BSS
14					0.18 to 1.0 mm; BSS
15					<0.18 mm; HMC
16					0.18 to 1.0 mm; HMC
17	24ARU-2004	Gum Creek	52.313559	-119.161888	<0.18 mm; BSS
18					0.18 to 1.0 mm; BSS
19					<0.18 mm; HMC
20					0.18 to 1.0 mm; HMC
21	24ARU-2005	Upper Fir	52.299607	-119.164953	<0.18 mm; BSS
22					0.18 to 1.0 mm; BSS
23					<0.18 mm; HMC
24					0.18 to 1.0 mm; HMC
25	24ARU-2006	Perry River	51.068451	-118.700786	<0.18 mm; BSS
26					0.18 to 1.0 mm; BSS
27					<0.18 mm; HMC
28					0.18 to 1.0 mm; HMC
29	24ARU-2007	Ratchford Creek	51.365787	-118.754744	<0.18 mm; BSS
30					0.18 to 1.0 mm; BSS
31					<0.18 mm; HMC
32					0.18 to 1.0 mm; HMC
33	24ARU-2008	Cranberry Creek	50.779047	-118.097014	<0.18 mm; BSS
34					0.18 to 1.0 mm; BSS
35					<0.18 mm; HMC
36					0.18 to 1.0 mm; HMC

BSS – bulk stream sediment; HMC – panned heavy mineral concentrate.

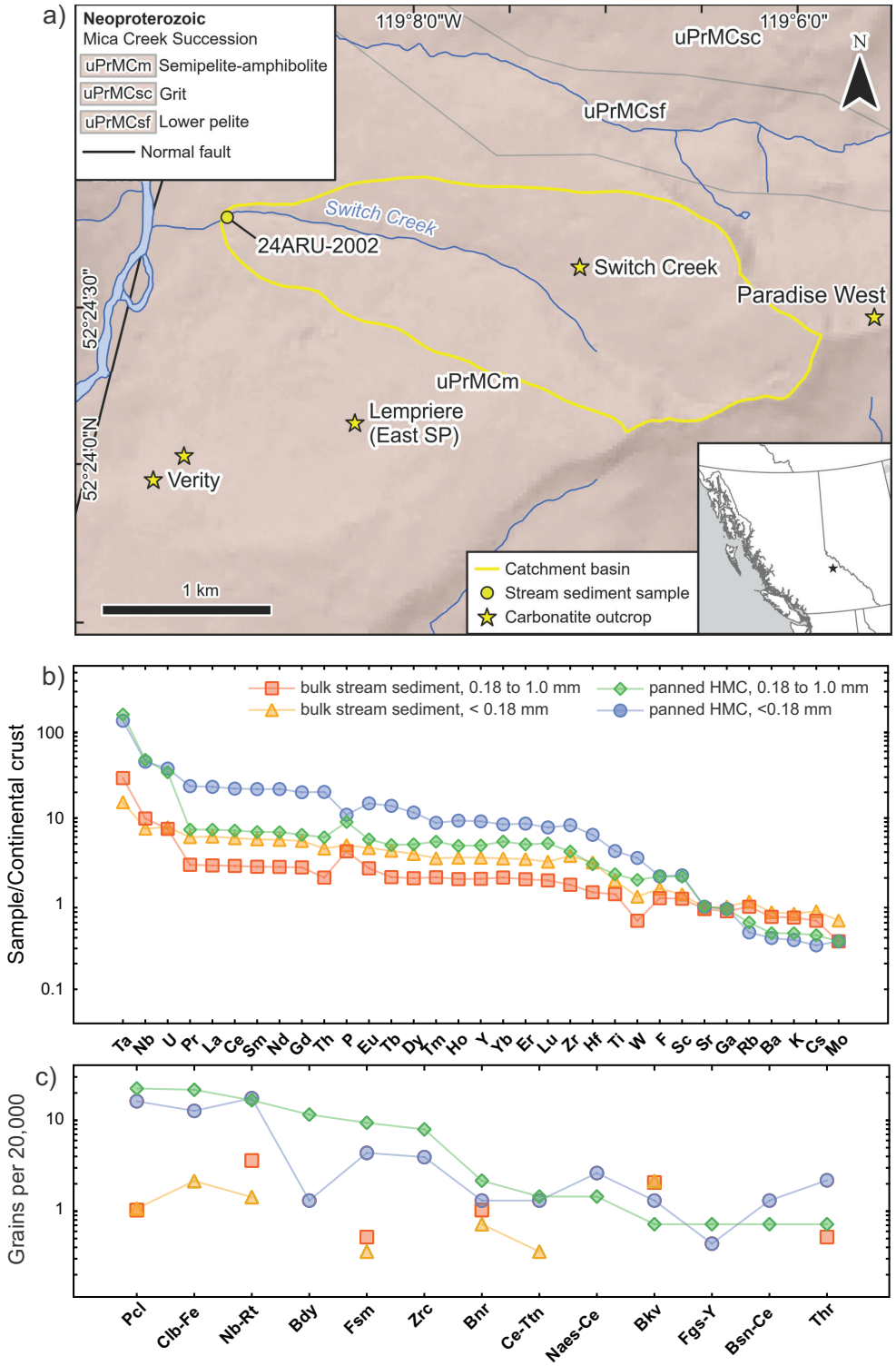

Fig. 2. a) Sampling site and catchment basin (area=3.17 km^2) at Switch Creek, downstream of Switch Creek carbonatite, Blue River area (83D/06). Carbonatite occurrences after Rukhlov et al. (2018). Geology after Campbell (1968), Simony et al. (1980), Raeside and Simony (1983), Pell and Simony (1987), McDonough et al. (1991, 1992), Murphy (2007), and British Columbia Geological Survey (2019). **b)** Bulk stream sediment and panned, heavy mineral concentrate (HMC) lithogeochemical data (Rukhlov et al., 2025b) normalized to bulk continental crust values of Rudnick and Gao (2014). **c)** Grain counts of indicator minerals in bulk stream sediment and panned, heavy mineral concentrate (HMC) per 20,000 total grains by scanning electron microscopy-mineral liberation analysis (SEM-MLA; Table 2); Mineral abbreviations (Warr, 2021): Bdy – baddeleyite, Bkv – belkovite, Bnr – brannerite, Bsn-Ce – bastnaesite-(Ce), Ce-Ttn – REE-titanite, Clb-Fe – columbite-(Fe), Fgs-Y – fergusonite-(Y), Fsm – fersmite, Naes-Ce – nioboaeschynite-(Ce), Nb-Rt – Nb-rutile, Pcl – pyrochlore supergroup, Thr – thorite, Zrc – zirconolite.

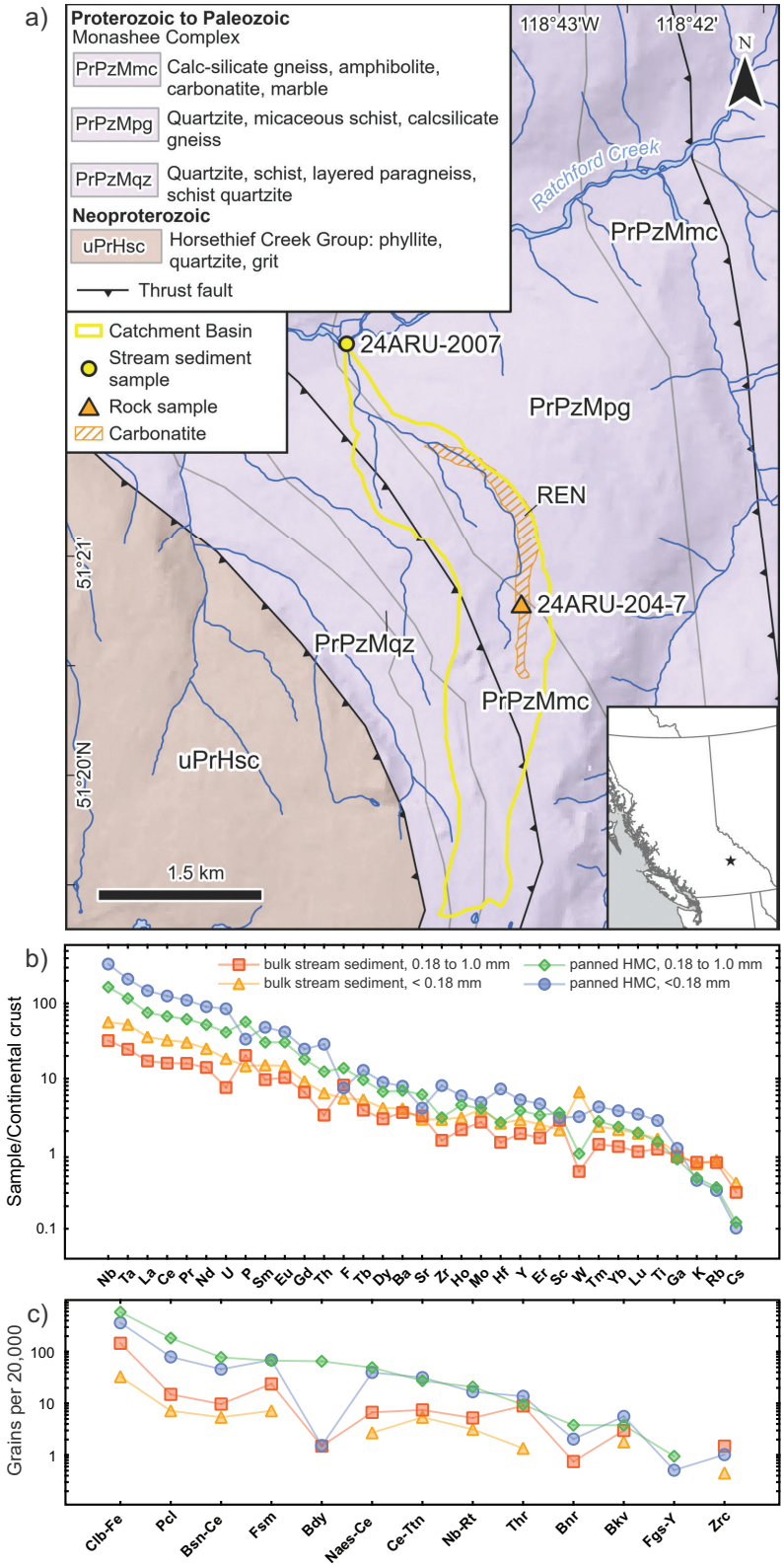

Fig. 3. a) Sampling sites and catchment basin (area=3.85 km^2) downstream of Ren (Ratchford Creek) carbonatite, Ratchford Creek valley (82M/07). Carbonatite footprint after Ya'acoby (2014). Geology after Wheeler and Fox (1964), Höy and Brown (1980), Logan (2002), and British Columbia Geological Survey (2019). **b)** Bulk stream sediment and panned, heavy mineral concentrate (HMC) lithogeochemical data (Rukhlov et al., 2025b) normalized to bulk continental crust values of Rudnick and Gao (2014). **c)** Grain counts of indicator minerals in bulk stream sediment and panned, heavy mineral concentrate (HMC) per 20,000 total grains by scanning electron microscopy-mineral liberation analysis (SEM-MLA; Table 2); Mineral abbreviations as in Figure 2c.

4.2. Mineral liberation analysis (MLA)

To generate mineral abundance maps and quantitative determinations, MLA was carried out using a FEI MLA 650 field emission gun SEM equipped with two Brucker silicon drift EDS detectors on the same grain mounts (normal sections) at the Core Research Equipment and Instrument Training (CREAIT) Microanalysis Facility (MAF), Memorial University of Newfoundland. Operating conditions for MLA included a 25 kV accelerating voltage and 10 nA current. Grain mounts were measured in XBSE (eXtended BackScattered Electron) mode where X-ray analyses were triggered for a backscattered electrons (BSE) range of 40 to 255. Each X-ray measurement was acquired for 0.012 seconds on a 1.5 by 1.5 mm or 2 by 2 mm frame, depending on the grain size (2 by 2 mm frame used for coarse-grained samples), with a resolution of 1000 pixels per frame and an imaging scan speed of 16 µs. Data reduction was performed on MLA Data View (FEI) software version 3.1.4.683.

Figure 4 shows typical EDS spectra for detrital rare-metal and REE minerals encountered in this study. Both QEMSCAN® and MLA scans produced consistent quantitative mineral abundances (Fig. 5). The value of MLA is the output of high-resolution, BSE and false-colour mineral maps, which were re-coloured using a Python™ script to highlight the minerals of interest (Fig. 6).

5. Micro X-ray fluorescence (µXRF) spectrometry

Elemental maps (Figs. 7, 8) were acquired using a Bruker TornadoPlus micro X-ray fluorescence (µXRF) instrument fitted with two 60 mm^2 detectors, housed in the Mineral Deposit Research Unit, University of British Columbia. Data were collected with a spatial resolution of 20 µm (generating images with a pixel resolution of 20 by 20 µm), with a counting time of 0.010 seconds per pixel, typically generating several thousand X-ray counts per pixel. Data were processed in Bruker ESPRIT® software. In the software, a colour stretch was applied to count data so that higher counts appear as brighter colors producing intensity maps. Interference and background corrections were applied, and concentrations calculated using a fundamental parameter (FP) method in Bruker ESPRIT® software. Because no standards were analyzed with our unknown samples, the results should be treated as semi-quantitative, with significant uncertainties at the level of individual pixels.

6. Detrital zircon analysis

Analytical details follow those documented in Ootes et al. (2022). Detrital zircons (Fig. 9) were separated from stream-sediment samples at the Pacific Centre for Isotopic and Geochemical Research at The University of British Columbia. Zircon crystals (>75 µm) were selected using conventional density and magnetic mineral-separation methods. The entire zircon separate was annealed at 900°C for 60 hours, then individual grains were hand-picked and mounted, polished, and imaged by cathodoluminescence (CL; Fig. 9b). From these images, grains were selected for isotopic analysis using a Resonetics RESOlution M-50-LR, connected via a Teflon squid to an Agilent 7700x quadrupole inductively coupled plasma mass spectrometer (ICP-MS). Pb/U and Pb/Pb ratios were determined on the same spots, along with trace-element concentration determinations (Fig. 9c). After data reduction, data were further screened using trace elements and concordance, and analytical results >6% discordant were removed (Fig. 9a).

7. Detrital apatite analysis

Apatite grains were recovered from bedrock carbonatite and stream-sediment samples (Rukhlov et al., 2025a) using conventional density and magnetic mineral-separation methods at the British Columbia Geological Survey. Modified analytical procedure generally follows that outlined in Mao et al. (2016, 2017). Individual grains were hand-picked, mounted, polished, and imaged by CL (Fig. 10a), BSE, and secondary electrons (SE) on a Hitachi SU3900 SEM equipped with dual Bruker XFlash7 30 mm^2 SDD energy-dispersive X-ray microanalysis system at the Electron Microbeam/Xray Diffraction Facility (EMXDF) at The University of British Columbia. A single electron probe micro-analysis (EPMA) was performed on each grain using a fully automated JEOL JXA-iHP200F field emission electron microprobe, equipped with five wavelength-dispersive spectrometers (WDS) at EMXDF. EPMA was performed using the WDS mode, accelerating voltage of 15 kV, beam current of 15 nA, and beam diameter of 10 µm.

Following the SEM and EPMA, apatite grains (n=436) were analyzed for 39 isotopes (Z=5 to 92) on an Agilent 8800 Triple Quadrupole ICP-MS/MS equipped with a Teledyne LSX-213 $G2^+$ laser ablation system at the School of Earth and Ocean Sciences, University of Victoria.

8. Discussion

8.1. Scanning electron microscopy

Samples downstream of both the Switch Creek and Ren (Ratchford Creek) carbonatites display significant enrichments in Ta, Nb, and REE relative to crust (Figs. 2b, 3b; Rukhlov et al., 2025a), reflecting the presence of detrital pyrochlore supergroup, columbite-(Fe), Nb-rutile, fersmite, nioboaeschynite-(Ce), bastnaesite-(Ce), zirconolite, and other carbonatite indicators (Fig. 6). These are relatively high-density minerals and thus are more abundant in panned HMC relative to bulk stream sediment (Figs. 2c, 3c). Both the <0.18 mm and 0.18 to 1.0 mm fractions show generally similar abundances of rare-metal and REE indicator minerals, except for baddeleyite (ZrO_2), which appears to concentrate in the coarse panned fraction. Although panned HMC is a preferred sample medium for rare-metal and REE (Rukhlov et al., 2024, 2025a), carbonatite indicator minerals were also detected in bulk stream-sediment samples (Tables 2, 3), suggesting the utility of automated mineralogy when applied to conventional RGS samples (<0.18 mm fraction of bulk stream sediment).

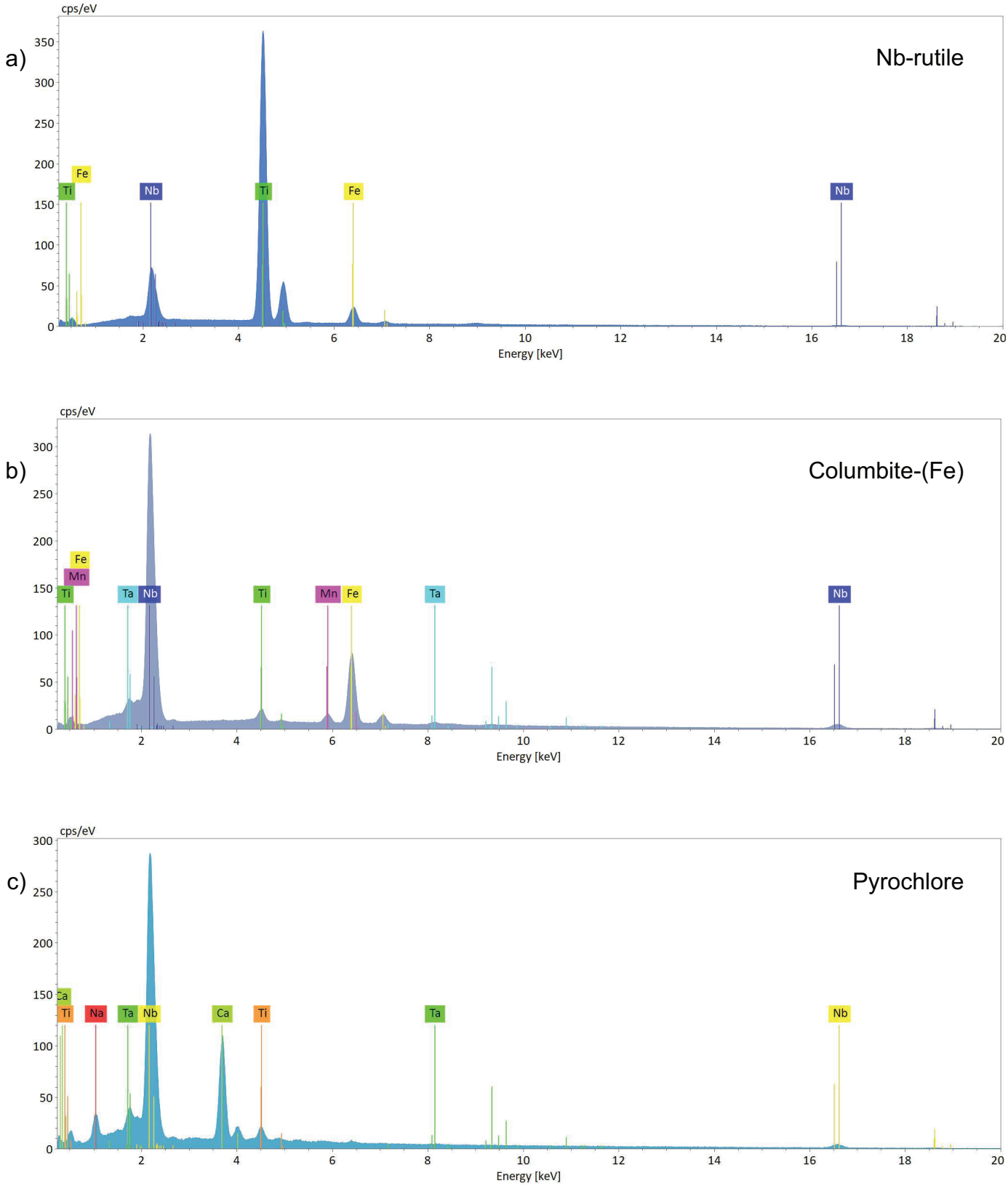

Fig. 4. Examples randomly picked from 36 sample set of X-ray energy dispersive spectra (EDS) for rare earth element (REE) and rare-metal minerals identified in stream-sediment samples. **a)** Nb-rutile. **b)** Columbite-(Fe). **c)** Pyrochlore.

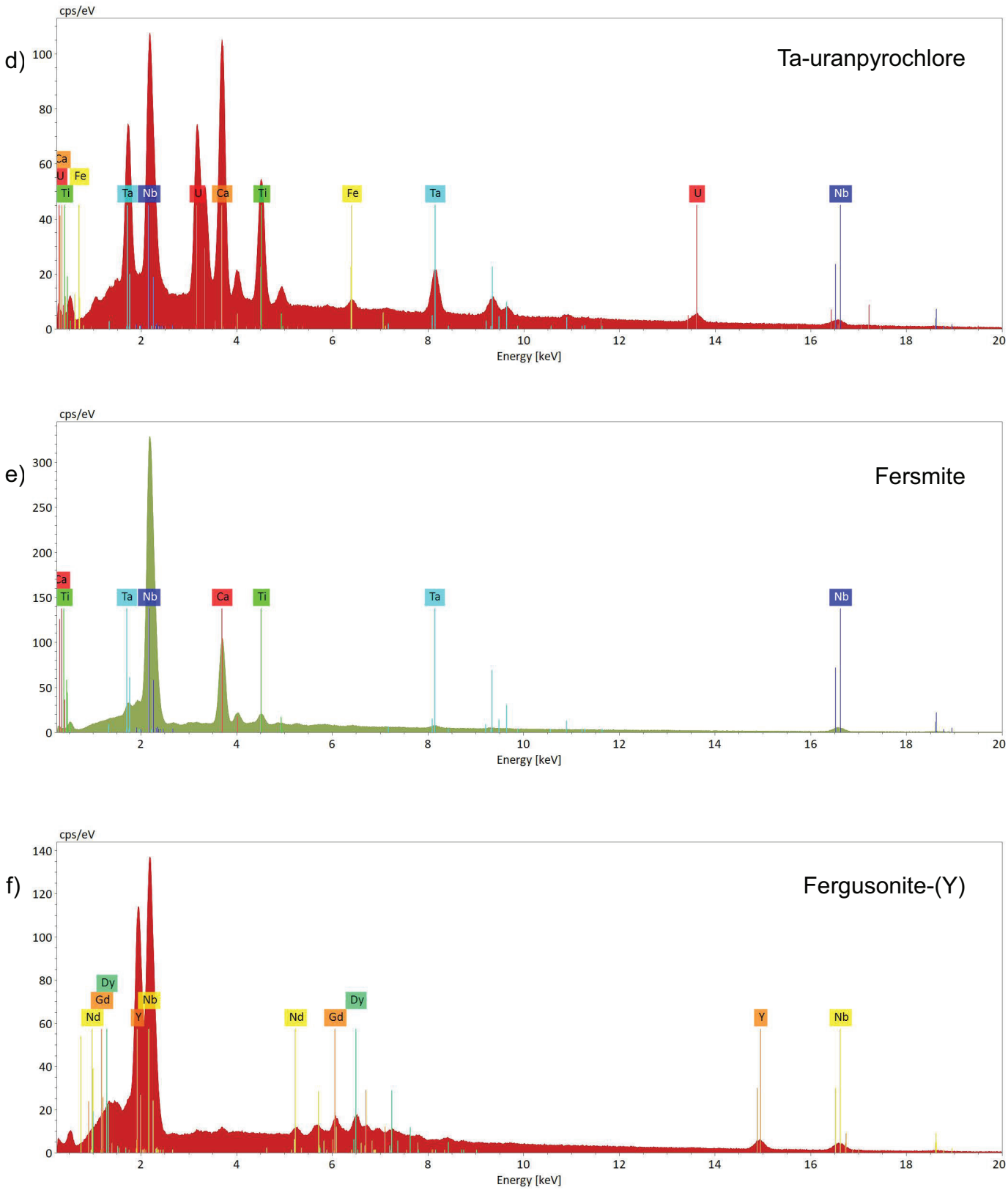

Fig. 4. Continued. **d)** Ta-uranpyrochlore. **e)** Fersmite. **f)** Fergusonite-(Y).

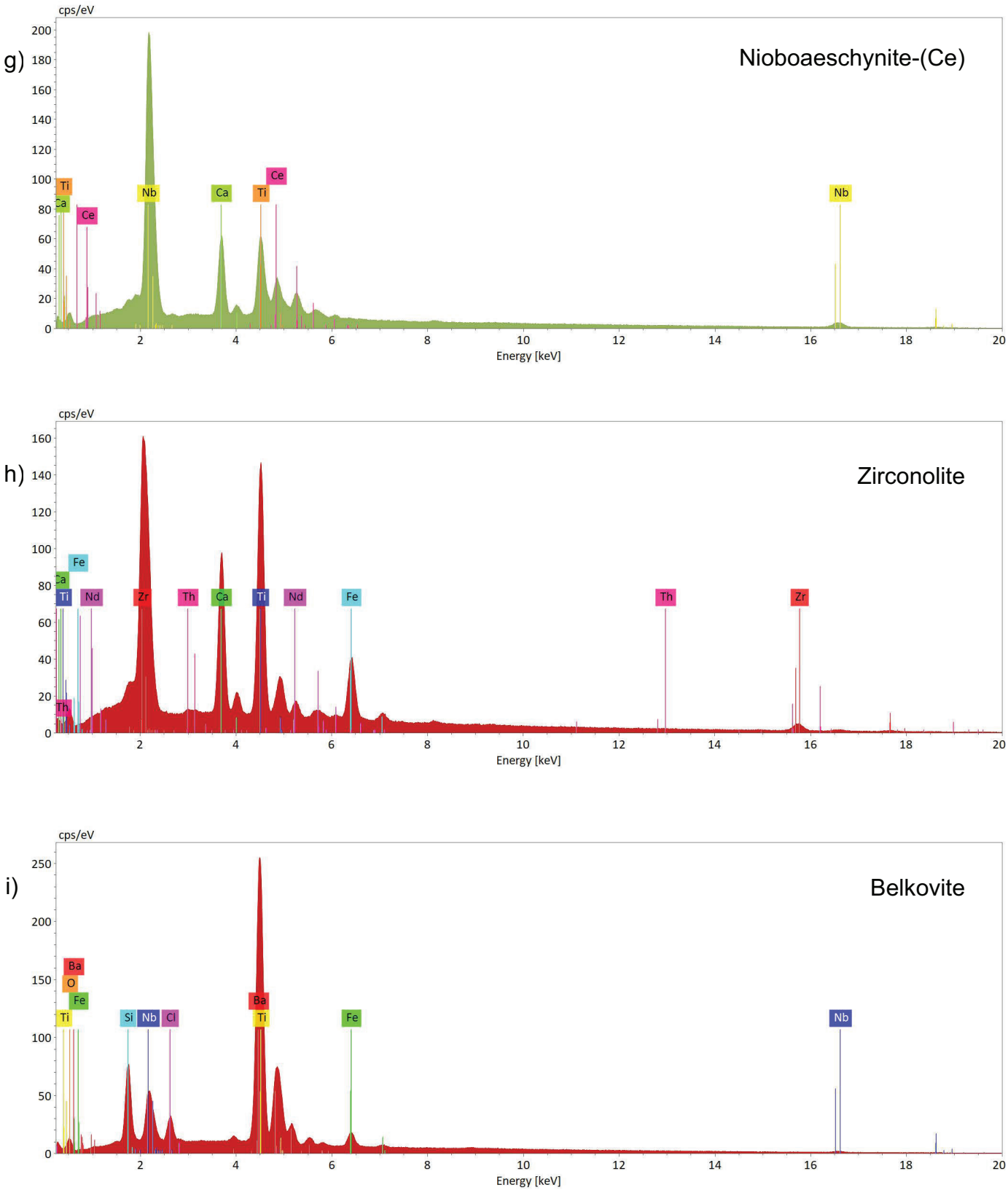

Fig. 4. Continued. **g)** Nioboaeschynite-(Ce). **h)** Zirconolite. **i)** Belkovite.

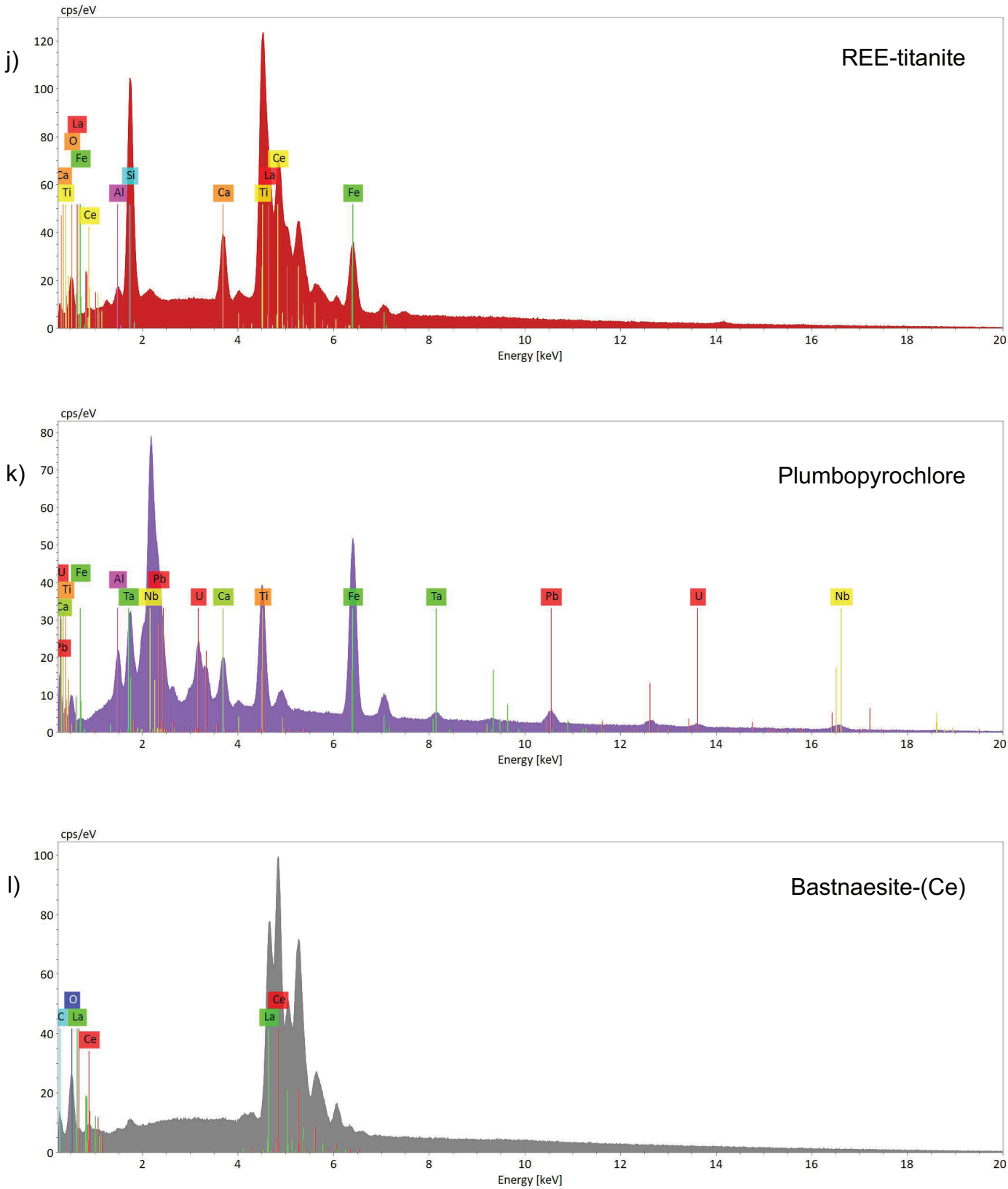

Fig. 4. Continued. **j)** REE-titanite. **k)** Plumbopyrochlore. **l)** Bastnaesite-(Ce).

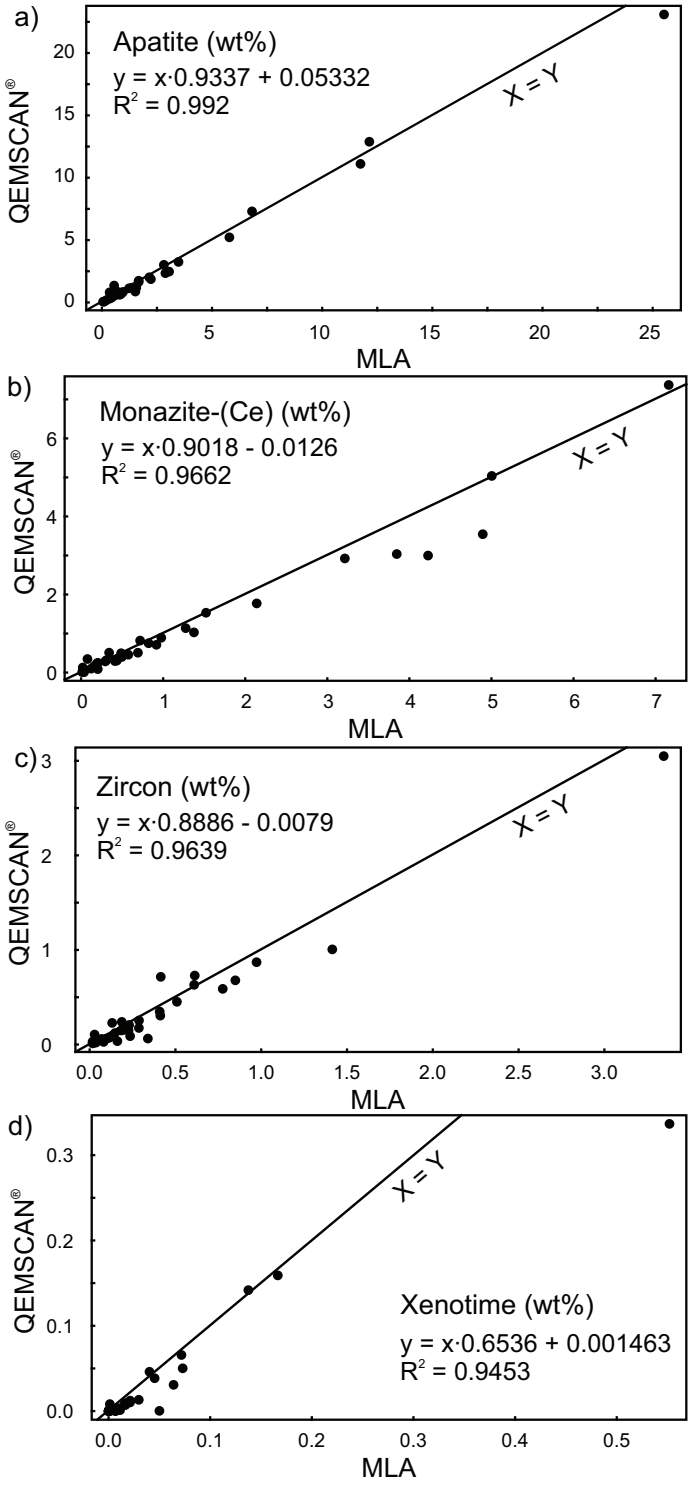

Fig. 5. Indicator mineral abundances in all 36 stream-sediment samples determined by mineral liberation analysis (MLA) vs. QEMSCAN®, ordinary least square regression equations, and correlation coefficients (R^2). **a)** Apatite (wt.%) by MLA vs. apatite (wt.%) by QEMSCAN®. **b)** Monazite-(Ce) (wt.%) by MLA vs. monazite-(Ce) (wt.%) by QEMSCAN®. **c)** Zircon (wt.%) by MLA vs. zircon (wt.%) by QEMSCAN®. **d)** Xenotime (wt.%) by MLA vs. xenotime (wt.%) by QEMSCAN®.

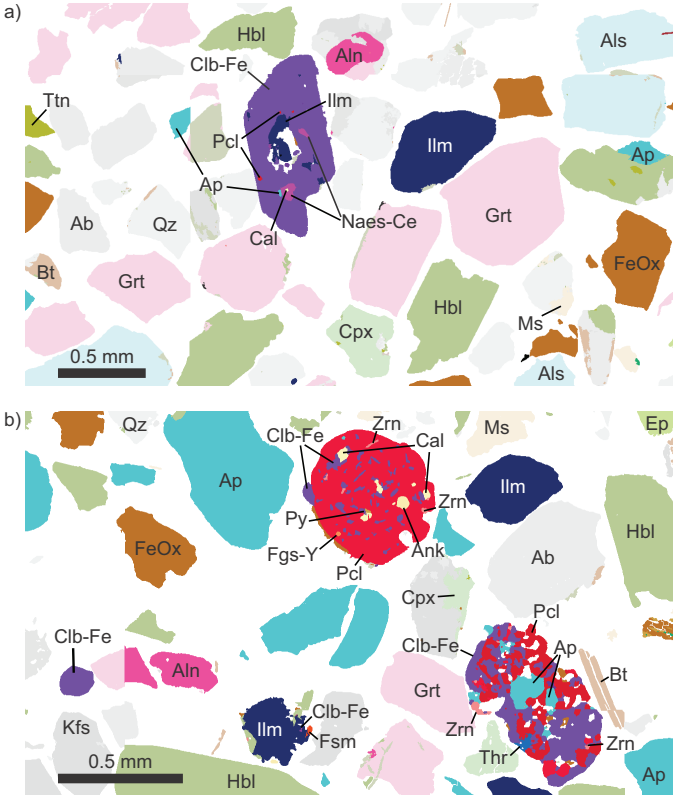

Fig. 6. Examples of false-colour, SEM-MLA maps of panned, heavy mineral concentrate (HMC) of stream sediment (0.18-1.0 mm fraction) in polished, 30 mm-diameter mounts. **a)** Sample 24ARU-2002; Switch Creek, downstream of Switch Creek carbonatite (Figure 2). **b)** Sample 24ARU-2007; tributary of Ratchford Creek, downstream of Ren (Ratchford Creek) carbonatite (Figure 3). Mineral abbreviations (Warr, 2021): Ab – albite, Aln – allanite, Als – aluminosilicate, Ank – ankerite, Ap – apatite, Bt – biotite, Cal – calcite, Clb-Fe – columbite-(Fe), Cpx – clinopyroxene, Ep – epidote, FeOx – iron oxide, Fgs-Y – fergusonite-(Y), Fsm – fersmite, Grt – garnet, Hbl – hornblende, Ilm – ilmenite, Kfs – K-feldspar, Ms – muscovite, Naes-Ce – nioboaeschynite-(Ce), Pcl – pyrochlore supergroup, Py – pyrite, Qz – quartz, Thr – thorite, Ttn – titanite, Zrn – zircon.

Detrital columbite, pyrochlore, and aeschynite could also be derived from pegmatites, syenites, and granites (e.g., Černý and Ercit, 2005; Dixon et al., 2014), which are more widespread than carbonatites in the study area, which is mostly underlain by high-grade metamorphic rocks. However, we consider that the presence of composite detrital particles such as columbite-pyrochlore-nioboaeschynite-ilmenite-apatite-calcite (Fig. 6a) or pyrochlore-columbite-zircon-fergusonite-ankerite-calcite-pyrite (Fig. 6b) parageneses unequivocally indicates the occurrence of carbonatites in the catchment basin upstream. Chemical compositions of detrital pyrochlore supergroup and other rare metal and REE minerals 'fingerprint' their host rocks (e.g., Mackay and Simandl, 2015; Simandl et al., 2017).

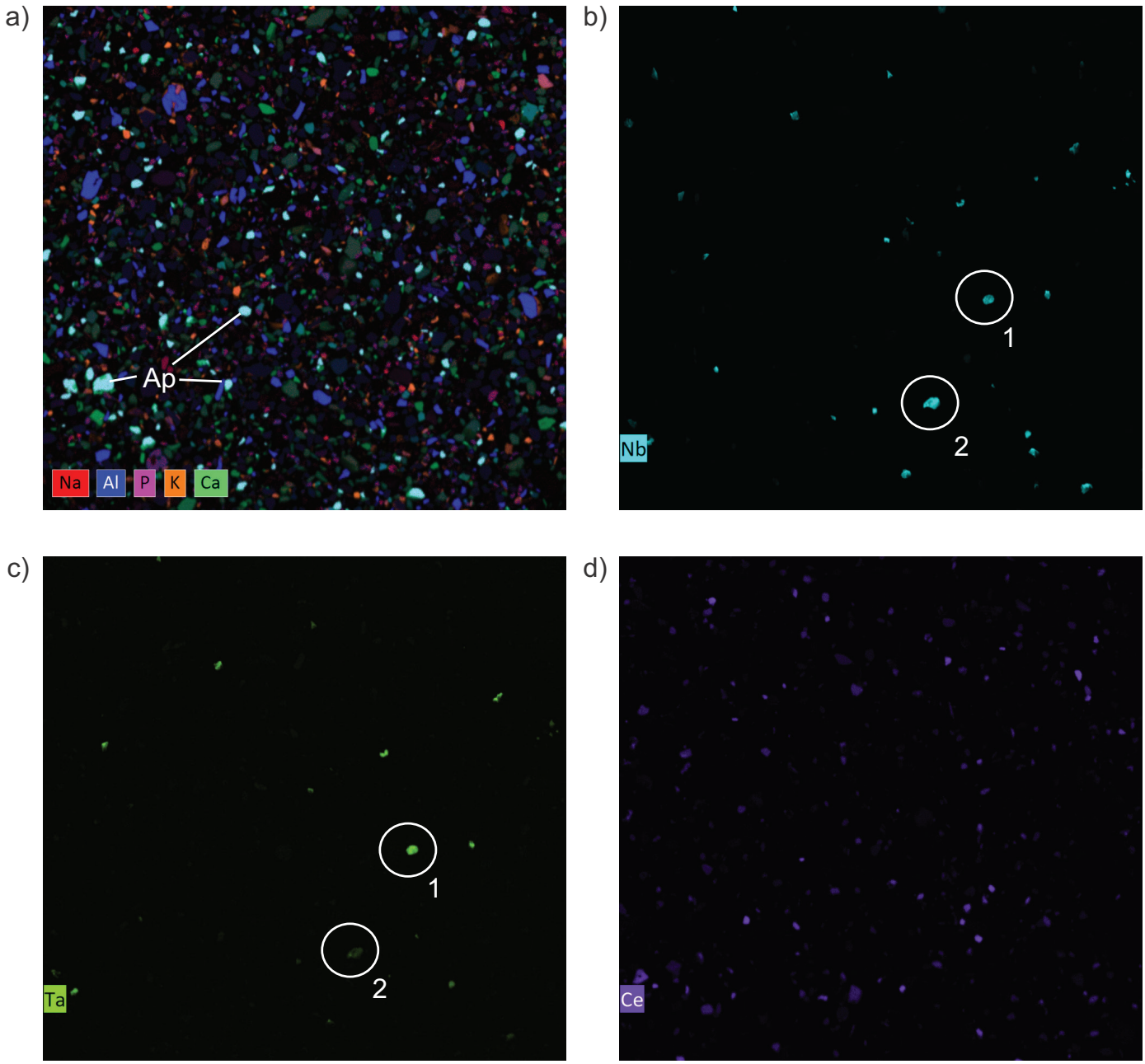

Fig. 7. Element intensity maps (21 by 21 mm area; count data) on polished, 30 mm-diameter mount of sample 24ARU-2002 collected downstream of Switch Creek carbonatite (Figure 2) by µXRF; brighter colours correspond to higher element intensity. **a)** Mixed Na-Kα, Al-Kα, P-Kα, K-Kα, and Ca-Kα; Ap - apatite. **b)** Nb-Kα. **c)** Ta-Lα. **d)** Ce-Lα. Note Ta-rich (circle 1) and Ta-poor (circle 2) Nb phases.

8.2. µXRF

Elemental maps derived from µXRF analysis highlight rare-metal and REE minerals and reveal compositional variations that are not apparent in MLA maps (Figs. 7, 8). For example, Ca and P highlight apatite, and variable Ta intensity differentiates Nb-Ta minerals downstream of Switch Creek and Ren carbonatites. High Ce counts highlight mainly detrital monazite-(Ce). Overall, µXRF is not an alternative to a much more powerful SEM-MLA approach but is a useful add-on to reveal compositional variations between indicator minerals.

8.3. Detrital zircon

The detrital zircons (Fig. 9a) reveal several distinct age populations ranging from Neoarchean to Eocene, including the 720, 530, and 330 Ma events marked by carbonatitic, alkaline, and mafic magmatism related to mantle-plume and rift activity (e.g., Heaman et al., 1992; Colpron et al., 2002; Lund et al., 2003; Millonig et al., 2012).

The trace-element compositions of zircons are sensitive to the petrogenesis and equilibrium mineral assemblage of their parental rock (e.g., Heaman et al., 1990; Grimes et al., 2007). These attributes make zircon a powerful indicator mineral for

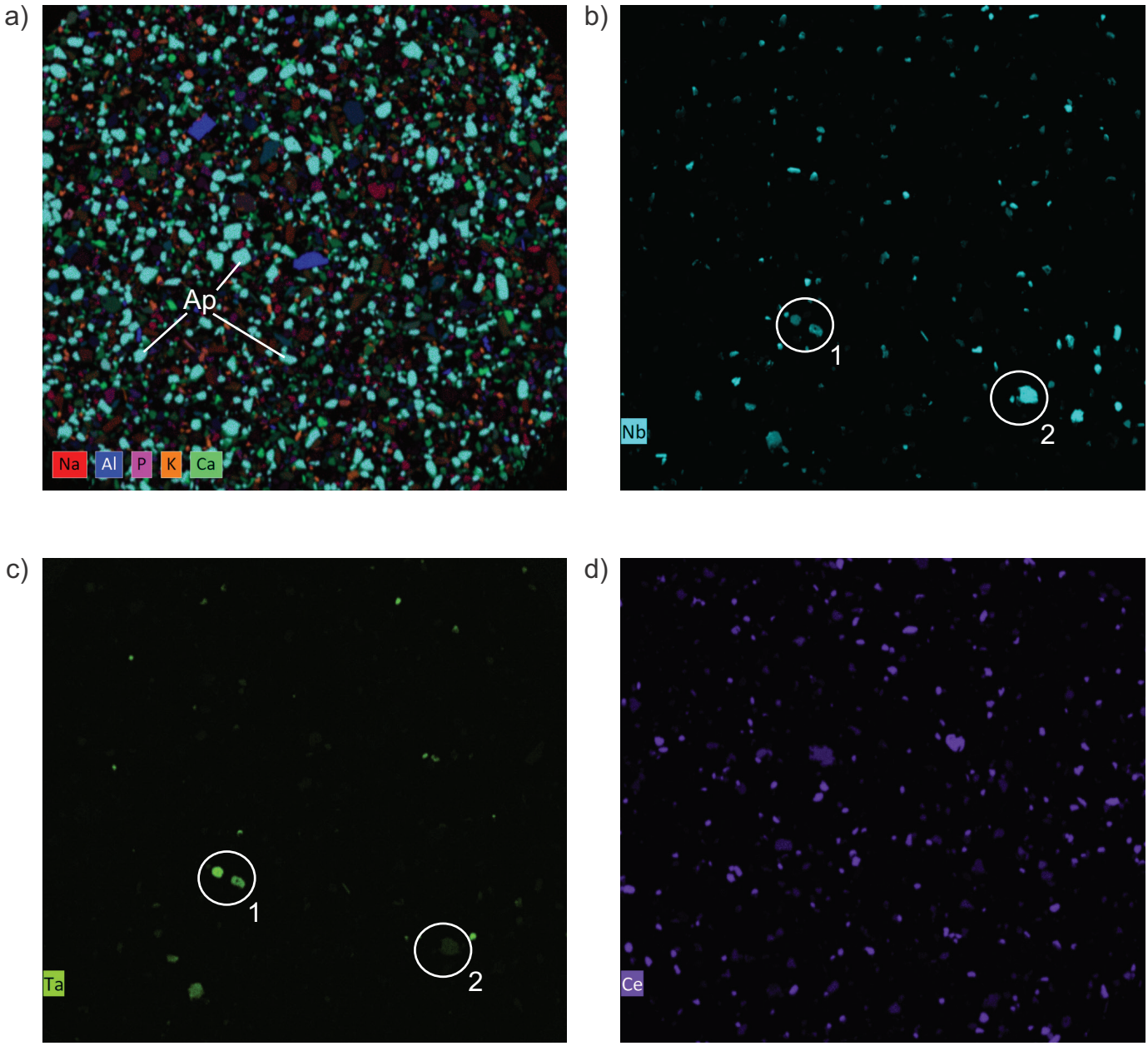

Fig. 8. Element intensity maps (21 by 21 mm area; count data) on polished, 30 mm-diameter mount of sample 24ARU-2007 collected downstream from Ren (Ratchford Creek) carbonatite (Figure 3) by µXRF; brighter colours correspond to higher element intensity. **a)** Mixed Na-Kα, Al-Kα, P-Kα, K-Kα, and Ca-Kα; Ap - apatite. **b)** Nb-Kα. **c)** Ta-Lα. **d)** Ce-Lα. Note Ta-rich (circle 1) and Ta-poor (circle 2) Nb phases.

identifying igneous source rocks, including kimberlites and carbonatites (Hardman et al., 2025). However, zircon is very rare in some carbonatites hosting REE and Nb (e.g., Dalsin et al., 2015; Gammons et al., 2024; Gary and Gammons, 2024), which limits its utility as an indicator mineral for carbonatite-hosted critical minerals.

Projected into the DPA discrimination diagram of Hardman et al. (2025), the trace-element compositions of the detrital zircon show most scatter defined by the <300 Ma population (Fig. 9c). A few Neoproterozoic to Carboniferous zircons plot within the field of carbonatites and related silica-undersaturated and alkaline rocks, and some 450 to 300 Ma zircons plot within the field of kimberlite and other low-volume 'kimberlite-like' rocks such as ultramafic lamprophyres.

8.4. Apatite

Apatite is ubiquitous in carbonatites and silica-undersaturated and alkaline silicate rocks (Kukharenko et al., 1965; Chakhmouradian et al., 2017; Rukhlov et al., 2018). Projected into the DPA discrimination diagram of Mao et al. (2016), the trace-element compositions of detrital apatite downstream from the Switch Creek (n=17) and Ren (n=21) carbonatites as well as those of apatite from other carbonatites in our total sample set (from Little Chicago, Felix, Ren, Three Valley Gap, and

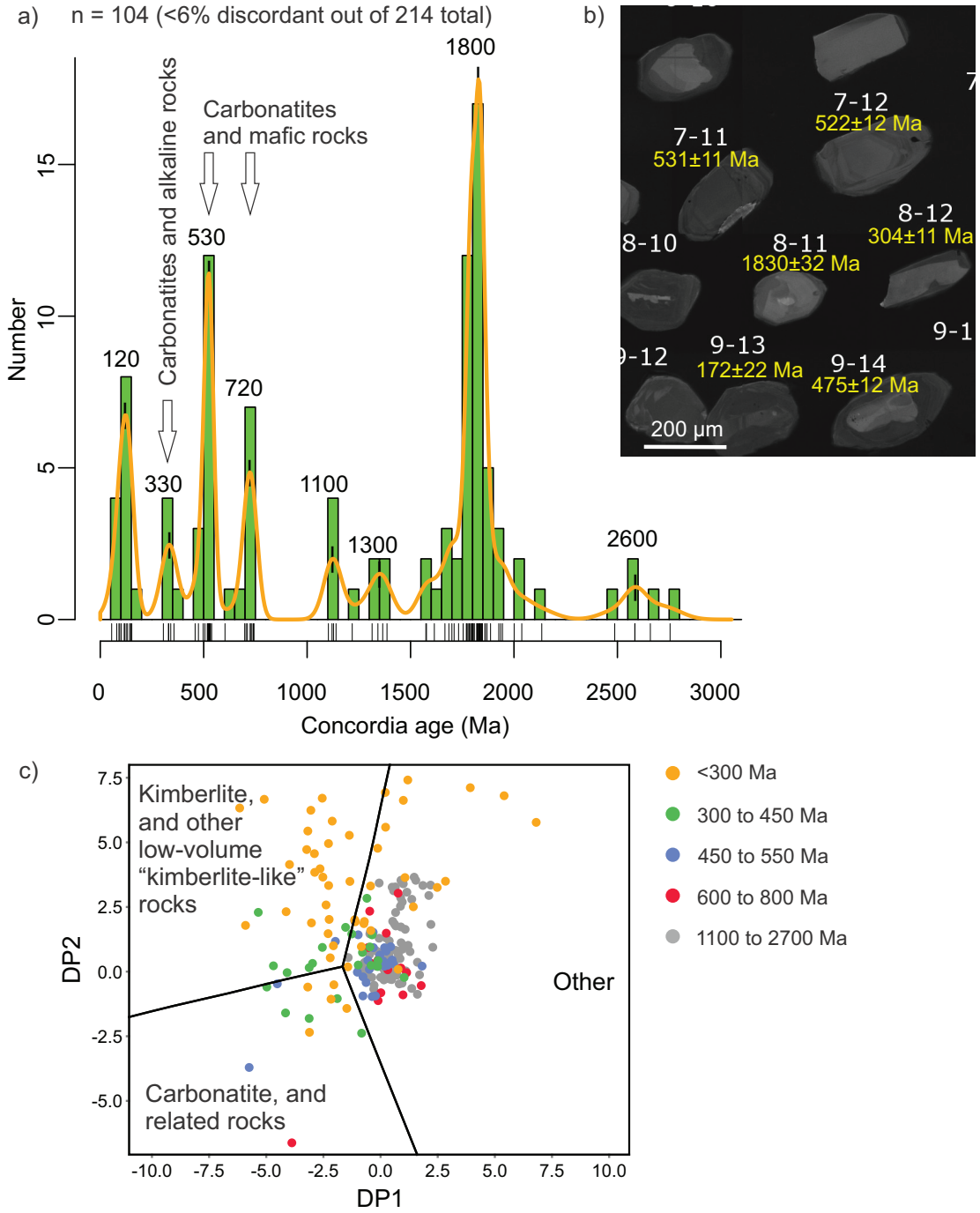

Fig. 9. LA-ICP-MS analyses of detrital zircons from stream sediment downstream of Switch Creek carbonatite, sample 24ARU-2002 (Figure 2). **a)** U-Pb concordia age (Ma) probability density plot showing the main probability age peaks. **b)** Examples of cathodoluminescence images of detrital zircons, showing their internal structures, and U-Pb concordia ages. **c)** Trace-element compositions of detrital zircons projected into DPA plot (after Hardman et al., 2025) based on 20 elemental variables.

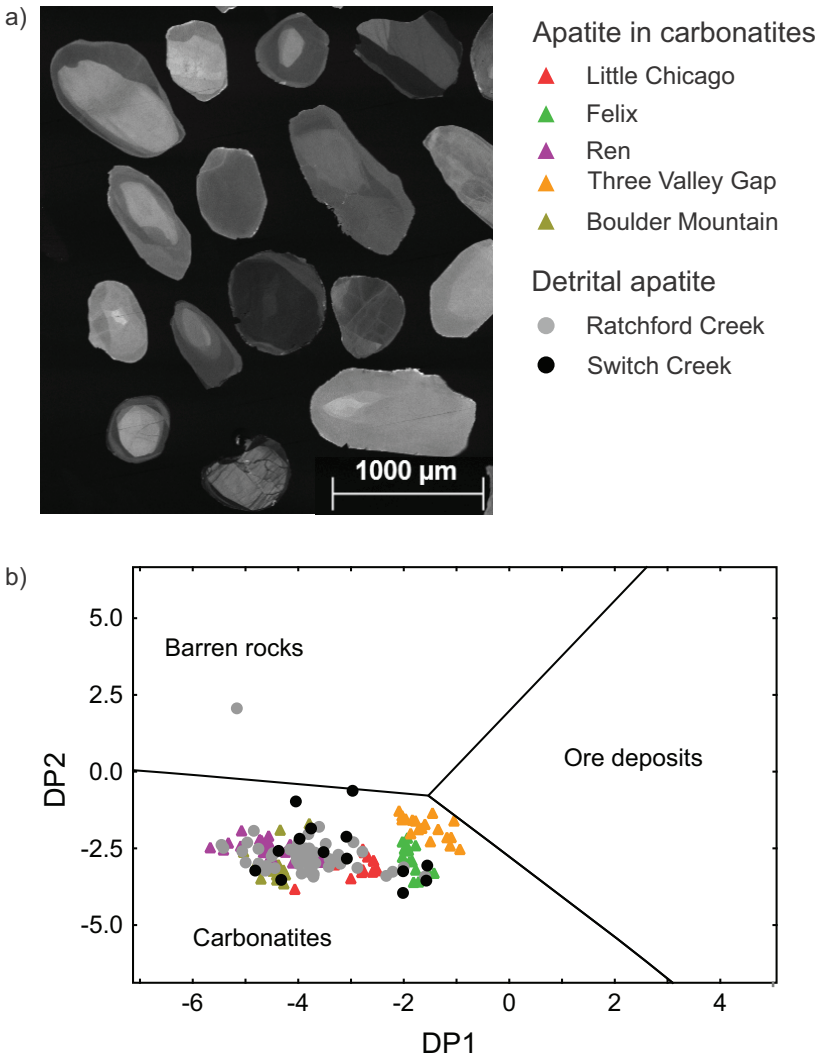

Fig. 10. a) Cathodoluminescence images of detrital apatite from stream sediment downstream of Ren (Ratchford Creek) carbonatite, sample 24ARU-2007 (Figure 3), showing their internal structures. **b)** LA-ICP-MS analyses of detrital apatite from stream sediments downstream of Switch Creek and Ren carbonatites, and apatite in some British Columbia carbonatites (see Rukhlov et al., 2025a for details) projected into DPA plot (after Mao et al., 2016) based on 11 elemental variables.

Boulder Mountain; see Rukhlov et al., 2025a) fall within the field of apatite compositions from global carbonatites (Fig. 10b). Considering that apatite is a common accessory mineral in most igneous and metamorphic rock, it is surprising that all detrital data points except one plot in the carbonatite field. This might reflect finer grain sizes (<0.18 mm) of non-carbonatitic apatite (cf., we used the 0.18 to 1.0 mm fraction for mineral separation), or a very low proportion of detrital apatite derived from local metamorphic rocks relative to ubiquitous, coarse-grained apatite sourced from the carbonatites (Rukhlov et al., 2018, 2025a).

Although we might have missed detrital apatite from other host rocks, the results downstream of both Switch Creek and Ren carbonatites are striking, because identifying even a single carbonatitic apatite grain in a stream sediment would render the catchment basin upstream prospective for carbonatites. It is interesting to note the clustering of data from individual carbonatite occurrences (Fig. 10b), reflecting compositional differences between the parental magmas. Our data confirm the utility of the approach used by Mao et al. (2016) in drainage prospecting for carbonatite-hosted critical minerals.

9. Conclusion

An indicator mineral approach using automated SEM mineralogy (QEMSCAN®, MLA), µXRF, and trace-element compositions of detrital zircon and apatite enhance the interpretation of multi-element lithogeochemical dispersal in modern drainages. Rare-metal and REE minerals concentrate in panned HMC, which display up to 100 times background (average continental crust) contrast, and is thus the preferred sample medium for ongoing REE, Nb, Ta, and other critical minerals prospecting. Our findings suggest that the approach

Table 2. Counts of mineral grains identified by scanning electron microscopy-mineral liberation analysis (SEM-MLA) in stream-sediment samples.

id	Total	Naes-Ce	Bdy	Aln	Bkv	Bnr	Clb-Fe	Fgs-Y	Fsm	Mnz-Ce	Pcl	Bsn-Ce	Nb-Rt	Thr	Ce-Ttn	Xtm
1	38040	nd	nd	167	7	3	6	nd	1	85	2	1	4	1	1	7
2	25075	3	nd	120	2	nd	4	nd	nd	42	3	nd	2	2	1	13
3	32707	nd	nd	168	3	nd	8	nd	2	197	12	1	3	2	nd	12
4	18496	nd	nd	89	9	1	6	nd	1	73	nd	nd	11	1	nd	16
5	55827	nd	nd	488	6	2	6	nd	1	34	3	nd	4	nd	1	7
6	38736	nd	nd	201	4	2	nd	nd	1	23	2	nd	7	1	nd	3
7	45661	6	3	414	3	3	29	1	10	149	37	3	40	5	3	13
8	27679	2	16	224	1	3	30	1	13	54	31	1	23	1	2	25
9	38018	nd	nd	196	nd	7	8	nd	nd	40	5	1	3	2	1	7
10	16319	nd	nd	84	4	2	3	nd	nd	21	nd	nd	3	1	nd	7
11	31577	nd	5	461	7	2	8	nd	2	179	10	nd	14	1	4	14
12	13863	nd	11	126	5	2	3	1	nd	42	2	nd	11	1	1	28
13	49938	1	nd	325	16	4	16	nd	nd	81	9	2	20	1	4	14
14	28946	nd	nd	221	4	2	11	nd	nd	19	2	nd	7	2	nd	3
15	33897	2	nd	318	14	4	16	1	nd	111	7	nd	23	3	9	15
16	21432	9	nd	279	30	3	255	nd	35	52	38	5	30	1	3	15
17	45791	2	nd	307	9	4	7	nd	2	151	6	3	11	nd	2	8
18	19308	nd	nd	98	1	3	2	nd	nd	30	3	2	8	nd	2	7
19	28392	10	nd	216	6	3	32	1	8	414	9	11	20	7	9	23
20	19618	10	nd	164	5	1	68	nd	6	123	9	8	38	1	11	34
21	58226	nd	nd	456	5	4	1	nd	nd	38	nd	nd	1	3	3	6
22	42190	nd	nd	271	8	1	4	1	nd	9	6	nd	4	1	1	5
23	43327	1	nd	513	5	4	24	1	nd	112	8	nd	8	1	7	17
24	31759	nd	nd	334	4	3	5	2	nd	19	2	nd	5	nd	1	6
25	43736	nd	nd	253	15	2	6	nd	nd	108	7	5	2	4	nd	2
26	19206	nd	nd	119	14	1	1	nd	nd	21	1	6	2	1	3	nd
27	31556	nd	2	392	9	1	4	nd	nd	422	8	8	4	2	5	9
28	17407	nd	nd	163	23	nd	nd	nd	nd	98	3	9	5	1	5	4
29	44465	6	nd	501	4	nd	73	nd	16	180	16	12	7	3	12	1
30	26774	9	2	292	4	1	195	nd	32	96	20	13	7	12	10	nd
31	39268	78	3	707	11	4	713	1	136	1101	156	90	33	27	62	7
32	21123	52	69	272	4	4	618	1	71	409	194	82	22	10	29	2
33	42762	nd	nd	137	10	1	1	nd	nd	61	1	1	8	nd	1	11
34	20967	nd	2	84	6	2	nd	nd	nd	21	nd	nd	8	nd	nd	4
35	31274	nd	nd	138	8	2	nd	nd	nd	845	nd	20	22	9	1	74
36	14925	nd	nd	75	6	nd	nd	nd	nd	44	1	2	8	2	nd	4

Table 2. Continued.

id	Zrc	Ap	Zrn	Cal	Ank	Ilm	Ti-Mag	Ttn	Ol	Cpx	Brt	Ab	Als	Apy	Bt	Ccp	Chl	Chr
1	nd	253	142	4	17	72	11	338	90	316	1	7790	576	nd	3448	nd	3812	8
2	nd	106	153	5	9	54	15	228	24	88	2	3414	232	nd	2566	nd	4494	8
3	nd	317	228	4	11	222	17	623	100	501	3	4621	941	nd	899	2	2295	16
4	nd	85	358	3	22	111	7	212	17	126	1	1480	384	nd	872	1	2794	63
5	nd	409	120	4	16	311	42	947	24	358	nd	6499	299	nd	6901	nd	7675	8
6	nd	284	152	nd	10	519	69	959	10	139	7	3021	218	nd	7091	1	7288	7
7	9	716	345	4	12	1098	186	1424	31	505	1	3347	735	nd	3837	nd	5116	16
8	11	306	326	3	22	845	144	615	36	200	nd	1487	333	nd	3451	3	5408	22
9	nd	348	131	1	16	245	3	341	13	125	nd	5089	446	nd	6458	14	2036	4
10	nd	100	210	4	12	108	3	243	12	42	1	1703	241	nd	2738	3	1561	7
11	4	709	440	4	27	713	55	837	39	180	nd	3021	1109	nd	1186	18	1307	15
12	2	116	494	6	8	410	54	269	21	39	nd	490	430	nd	737	7	1556	40
13	nd	122	113	nd	15	407	90	567	144	319	nd	8062	410	nd	4886	nd	8165	10
14	nd	76	125	1	8	142	19	566	7	82	1	3438	104	nd	4277	nd	5713	9
15	nd	138	163	nd	25	604	104	709	146	306	nd	4722	592	nd	2525	nd	4006	42
16	nd	56	207	1	22	353	70	346	30	160	2	1841	399	1	2350	nd	4197	44
17	nd	257	115	3	19	273	15	295	27	207	5	6176	536	nd	8743	1	5259	37
18	nd	49	105	4	9	169	10	125	3	95	1	1662	183	nd	4351	1	3655	29
19	nd	263	260	3	26	577	56	321	23	211	37	2844	1178	nd	2547	nd	3042	79
20	nd	63	379	4	26	391	45	158	12	102	53	949	592	nd	2657	nd	4257	200
21	nd	59	70	nd	24	163	42	440	331	257	2	7654	141	nd	4852	nd	14031	36
22	1	51	105	nd	21	101	13	484	558	156	nd	4543	99	nd	3943	nd	10668	65
23	nd	110	159	1	34	556	97	873	803	620	nd	5116	425	nd	2132	nd	6905	118
24	nd	75	111	1	19	180	64	424	585	264	1	2827	164	nd	2040	nd	7484	109
25	nd	650	121	3	13	141	58	305	51	612	nd	9186	172	nd	2790	nd	5212	6
26	nd	220	69	5	20	93	144	260	9	146	nd	3325	40	nd	1232	1	2837	17
27	1	1208	455	5	24	462	123	514	76	945	5	5253	123	nd	935	4	2389	7
28	nd	255	130	5	46	211	80	220	19	270	nd	2311	113	nd	1105	2	2517	24
29	1	1095	77	24	1041	236	58	326	73	1599	61	5984	105	nd	5365	2	5390	30
30	2	655	115	27	248	239	27	384	58	870	19	3618	16	nd	3559	1	3075	17
31	2	2602	359	51	957	1226	240	657	108	2596	323	3469	195	nd	2036	6	2285	48
32	nd	1337	190	50	297	571	84	288	36	820	84	1746	53	nd	1770	5	1873	60
33	nd	170	136	2	18	111	25	236	278	780	1	6667	357	1	3497	2	2744	5
34	nd	84	101	1	5	55	9	116	27	105	nd	3424	137	nd	2172	3	1673	9
35	1	365	426	5	29	575	92	441	592	1508	4	3517	289	1	1153	5	1173	33
36	nd	68	124	3	21	126	23	196	112	398	nd	1677	225	1	1102	5	1135	19

Table 2. Continued.

id	Ep	Gn	Grt	Hbl	FeOx	Ms	Kfs	Pl	Py	Qz	Rsv	Rt	Sch	Sp	St	Crn	X
1	385	3	1932	3691	450	2834	2543	1086	10	7652	38	86	nd	1	166	nd	nd
2	276	1	1022	2031	442	2490	2315	425	13	4127	57	82	nd	2	199	nd	3
3	383	nd	4113	4094	190	603	1692	712	20	9300	16	150	2	2	221	nd	1
4	143	nd	2324	1540	316	523	703	228	54	5639	16	120	nd	nd	145	nd	2
5	572	nd	1849	6286	398	4646	3436	1376	8	12294	101	120	nd	nd	569	nd	7
6	370	2	2009	2810	692	2784	2920	545	27	5718	182	164	nd	nd	491	nd	3
7	764	2	4893	4555	1628	1389	2197	613	22	10389	96	449	nd	nd	546	nd	17
8	403	nd	3346	1553	1477	1331	1592	231	12	3234	50	244	nd	nd	553	nd	14
9	675	nd	1514	2972	549	3541	1024	2030	199	9407	270	146	nd	1	150	nd	nd
10	257	1	874	1194	232	1094	659	611	84	3669	166	219	nd	nd	143	nd	3
11	801	1	5540	4089	689	424	514	1320	231	6540	174	674	nd	1	207	nd	1
12	143	nd	2322	833	484	282	168	231	84	3726	53	471	nd	nd	150	nd	4
13	315	nd	1550	5795	485	3622	3141	1130	7	9249	120	118	1	nd	600	nd	2
14	150	nd	1292	2489	421	2124	3956	362	3	2618	167	50	nd	nd	473	nd	2
15	257	nd	1854	4694	555	1244	2141	594	28	7273	88	170	nd	nd	390	1	4
16	198	2	1231	2118	458	1191	1515	274	12	2893	77	131	nd	nd	491	nd	7
17	324	nd	1355	4159	287	4699	1552	1040	28	9028	144	93	nd	nd	599	nd	3
18	187	nd	1329	1025	291	1557	765	346	10	2560	114	54	nd	nd	462	nd	1
19	257	nd	3638	1944	468	848	407	704	26	6834	155	312	3	nd	551	nd	9
20	69	nd	1932	891	482	893	291	230	29	3393	151	263	nd	1	623	nd	4
21	426	1	2493	8723	413	3830	3280	1318	10	7642	126	45	nd	nd	1300	nd	nd
22	319	1	1634	5957	715	2358	4432	762	4	3808	128	78	nd	nd	872	nd	3
23	378	nd	2618	7736	612	1447	2535	838	5	7588	84	152	nd	nd	680	1	4
24	318	nd	1707	5342	508	1537	2702	365	3	3673	125	72	nd	1	670	nd	5
25	427	nd	801	3369	434	2201	6285	1867	14	7363	14	104	nd	nd	1132	2	1
26	253	nd	389	1416	263	1883	3020	490	15	2164	6	132	nd	1	586	nd	1
27	415	nd	1445	2811	1199	1428	3588	1173	53	5333	12	106	4	nd	594	13	nd
28	215	nd	683	1295	619	1404	2144	410	32	2024	38	151	nd	nd	768	3	5
29	446	nd	1890	7135	1543	1244	3417	1471	142	4333	91	61	nd	3	389	nd	2
30	276	nd	847	3802	911	924	3870	680	54	1508	32	38	nd	nd	207	nd	2
31	353	1	2142	4889	3898	628	2396	878	254	3195	100	104	1	2	132	1	6
32	125	5	992	2675	1637	683	1897	362	77	1343	39	71	nd	4	100	nd	10
33	421	nd	389	2391	436	3200	7095	866	40	11778	12	137	nd	2	722	nd	11
34	244	nd	193	719	323	2670	3888	312	14	4024	9	99	nd	nd	419	nd	5
35	313	1	2166	2270	744	1543	3569	509	56	8169	10	244	1	1	341	nd	9
36	177	1	524	728	195	1541	2051	242	16	3568	5	127	nd	nd	353	nd	20

Total – total count of grains; 'nd' – not detected; X – unknown phase. Mineral abbreviations (Warr, 2021): Ab – albite, Aln – allanite, Als – aluminosilicate, Ank – ankerite, Ap – apatite, Apy – arsenopyrite, Bdy – baddeleyite, Bkv – belkovite, Bnr – brannerite, Bsn Ce – bastnaesite-(Ce), Brt – baryte, Bt – biotite, Cal – calcite, Ccp – chalcopyrite, Ce-Ttn – REE-titanite, Chl – chlorite, Chr – chromite, Clb-Fe – columbite-(Fe), Cpx – clinopyroxene, Crn – corundum, Ep – epidote, FeOx – iron oxide, Fgs-Y – fergusonite-(Y), Fsm – fersmite, Gn – galena, Grt – garnet, Hbl – hornblende, Ilm – ilmenite, Kfs – K-feldspar, Mnz-Ce – monazite-(Ce), Ms – muscovite, Naes Ce – nioboaeschynite-(Ce), Nb-Rt – Nb-rutile, Ol – olivine, Pcl – pyrochlore supergroup, Pl – plagioclase, Py – pyrite, Qz – quartz, Rsv – rasvumite, Rt – rutile, Sch – scheelite, Sp – sphalerite, St – staurolite, Thr – thorite, Ti-Mag – Ti-magnetite, Ttn – titanite, Zrc – zirconolite, Zrn – zircon, Xtm – xenotime.

Table 3. Detrital indicator minerals identified in stream sediments by scanning electron microscopy-mineral liberation analysis (SEM-MLA).

Mineral	General formula	Significance
Bastnaesite-(Ce)	$(Ce,La)(CO_3)(F)$	REE
Nioboaeschynite-(Ce)	$(Ce,Ca)(Nb,Ti)_2(O,OH)_6$	REE, Nb
Baddeleyite	ZrO_2	Carbonatites, undersaturated and alkaline silicate rocks
Brannerite	$(U,Ce,Th,Ca)(Ti,Fe^{3+},Nb)_2(O,OH)_6$	REE, Nb
Columbite-(Fe)	$(Fe^{2+},Mn)(Nb,Ta)_2O_6$	Nb ±Ta
Fergusonite-(Y)	$YNbO_4$	REE, Nb
Fersmite	$(Ca,Ce,Na)(Nb,Ta,Ti)_2(O,OH,F)_6$	REE, Nb ±Ta
Nb-rutile	$(Ti,Nb)O_2$	Nb
Thorite	$Th(SiO_4)$	Alkaline rocks, pegmatites
Pyrochlore	$(Ca,Na,U,Fe,Pb)_2(Nb,Ta,Ti)_2O_6(F,OH,O)$	Nb ±Ta
Zirconolite	$(Ca,Nd)Zr(Ti,Fe,Th)_2O_7$	REE
Apatite	$Ca_5(PO_4)_3(F,Cl,OH)$	Abundant in carbonatites; indicator chemistry[1]
Monazite-(Ce)	$Ce(PO_4)$	REE
Xenotime	$Y(PO_4)$	REE
Allanite-(Ce)	$(Ca,Ce)_2(Al,Fe)_3(Si_2O_7)(SiO_4)O(OH)$	REE
Belkovite	$Ba_3(Nb,Ti,Fe)_6(Si_2O_7)_2O_{12}$	Nb
REE-titanite	$(Ca,Ce,La)(Ti,Al)(SiO_4)O$	REE
Zircon	$Zr(SiO_4)$	Occurs in carbonatites; indicator chemistry[2]

[1] Mao et al. (2016). [2] Hardman et al. (2025). REE - rare earth elements.

also suits small volume (~2 g), bulk stream-sediment samples in the RGS archive. In addition to identifying new critical mineral targets, data from indicator minerals inform tectonic evolution, geology, and metallogeny of the catchment basins.

Acknowledgments

We are grateful to K. Whitmore (BC Geological Survey) for building a script for re-processing MLA images. We thank E. Hrischeva (Activation Laboratories Ltd.) for analytical services and Christopher H. Gammons (Montana Technological University) and Lawrence B. Aspler (BC Geological Survey) for thorough reviews and helpful comments.

References cited

British Columbia Geological Survey, 2019. British Columbia Digital Geology. British Columbia Ministry of Mining and Critical Minerals, British Columbia Geological Survey. Data version 2019-12-19. <https://www2.gov.bc.ca/gov/content/industry/mineral-exploration-mining/british-columbia-geological-survey/geology/bcdigitalgeology>

Campbell, R.B., 1968. Geology, Canoe River, British Columbia. Geological Survey of Canada Preliminary Map 15-1967, 1:253,400 scale.

Černý P., and Ercit, T.S., 2005. The classification of granitic pegmatites revisited. The Canadian Mineralogist, 43, 2005-2026.

Chakhmouradian, A.R., Reguir, E.P., Zaitsev, A.N., Couëslan, C., Xu, C., Kynický, J., Mumin, A.H., and Yang, P., 2017. Apatite in carbonatitic rocks: Compositional variation, zoning, element partitioning and petrogenetic significance. Lithos, 274-275, 188-213.

Colpron, M., 2020. Yukon terranes-A digital atlas of terranes for the northern Cordillera. Yukon Geological Survey. <https://data.geology.gov.yk.ca/Compilation/2#InfoTab>

Colpron, M., Logan, J.M., and Mortensen, J.K., 2002. U-Pb zircon age constraint for late Neoproterozoic rifting and initiation of the lower Paleozoic passive margin of western Laurentia. Canadian Journal of Earth Sciences, 39, 133-143.

Dalsin, M.L., Groat, L.A., Creighton, S., and Evans, R.J., 2015. The mineralogy and geochemistry of the Wicheeda carbonatite complex, British Columbia, Canada. Ore Geology Reviews, 64, 523-542.

Dixon, A., Cempírek, J., and Groat, L.A., 2014. Mineralogy and geochemistry of pegmatites on Mount Begbie, British Columbia. The Canadian Mineralogist, 52, 129-164.

Gammons, C.H., Risedorf, S., Wyss, G., and Lowers, H., 2024. Occurrences of the rare, REE minerals daqingshanite, törnebohmite, biraite, sahamalite, and ferriperbøeite from the Sheep Creek area, Montana, USA. Minerals 14, article1047. <https://doi.org/10.3390/min14101047>

Gary, M.A., 2024. Using indicator minerals from stream sediment samples to detect rare earth element deposits. Unpublished M.Sc. thesis, Montana Technological University, Butte, MT, USA, 80 p. <https://digitalcommons.mtech.edu/grad_rsch/321>

Gary, M.A., and Gammons, C.H., 2024. Using indicator minerals from stream sediment samples to detect rare earth element deposits. In: Van Rythoven, A., and Barth, S., (Eds.), Proceedings of the Montana Mining and Mineral Symposium 2023, September 27-30, 2023, Butte, Montana, Montana Bureau of Mines and Geology, Special Publication 124, pp. 53-58. <https://mbmg.mtech.edu/pdf-publications/SP124.pdf>

Grimes, C.B., John, B.E., Kelemen, P.B., Mazdab, F.K., Wooden, J.L., Cheadle, M.J., Hanghoj. K., and Schwartz, J.J., 2007. Trace element chemistry of zircons from oceanic crust: a method for distinguishing detrital zircon provenance. Geology, 35, 643-646. <https://doi.org/10.1130/G23603A.1>

Hardman, M.F., Pearson, D.G., DuFrane, S.A., Cabral Neto, I., Azzone, R.G., Shu, Q., Hinde, J., and Rukhlov, A.S., 2025. Improved trace element discrimination of kimberlitic and carbonatitic zircon: implications for zircon origin in kimberlite and the search for superdeep diamonds. Mineralogy and Petrology, 119, 583-605. <https://doi.org/10.1007/s00710-025-00916-2>

Heaman, L.M., Bowins, R., and Crocket, J., 1990. The chemical composition of igneous zircon suites: implications for geochemical tracer studies. Geochimica et Cosmochimica Acta, 54, 1597-1607.

Heaman, L., LeCheminant, A., and Rainbird, R.H., 1992. Nature and timing of Franklin igneous events, Canada: implications for a late Proterozoic mantle plume and the break–up of Laurentia. Earth and Planetary Science Letters, 109, 117-131.

Höy, T., and Brown, R.L., 1980. Geology of the eastern margin of Shuswap Complex, Frenchman Cap area. British Columbia Ministry of Energy, Mines and Petroleum Resources, British Columbia Geological Survey Preliminary Map 43, 1:100,000 scale.

Kukharenko, A.A., Orlova, M.P., Bulakh, A.G., Bagdasarov, E.A., Rimskaya-Korsakova, O.M., Nefedov, E.I., Ilynsky, G.A., Sergeev, A.S., and Abakumova, N.B., 1965. Caledonian complex of ultrabasic, alkaline rocks, and carbonatites of the Kola Peninsula and Northern Karelia (Geology, Petrology, Mineralogy, and Geochemistry). Nedra, Moscow, 772 p.

Kulla, G., and Hardy, J., 2015. Commerce Resources Corp. Blue River tantalum-niobium project, British Columbia, Canada, project update report. NI 43-101 Technical Report, 138 p. <https://www.sedarplus.ca/csfsprod/data151/filings/02317786/00000003/C%3A%5CFILINGS%5CSEDAR%5CCommerce%5CCCE_tech_rpt_031815.pdf>

Logan, J.M., (compiler), 2002. Intrusion-related mineral occurrences of the Cretaceous Bayonne magmatic belt, southeast British Columbia. British Columbia Ministry of Energy and Mines, British Columbia Geological Survey Geoscience Map 2002-01, 1:500,000 scale.

Lund, K., Aleinikoff, J.N., Evans, K.V., and Fanning, C.M., 2003. SHRIMP U-Pb geochronology of Neoproterozoic Windermere Supergroup, central Idaho: Implications for rifting of western Laurentia and synchroneity of Sturtian glacial deposits. Geological Society of America Bulletin, 115, 349-372.

Mackay, D.A.R., and Simandl, G.J., 2015. Pyrochlore and columbite-tantalite as indicator minerals for specialty metal deposits. Geochemistry: Exploration, Environment, Analysis, 15, 167-178.

Mäder, U.K., 1987. The Aley carbonatite complex, northern Rocky Mountains, British Columbia (94B/5). In: Geological Fieldwork 1986, British Columbia Ministry of Energy, Mines and Petroleum Resources, British Columbia Geological Survey Paper 1987-1, pp. 283-288.

Mao, M., Rukhlov, A.S., Rowins, S.M., Spence, J., and Coogan, L.A., 2016. Apatite trace element compositions: A robust new tool for mineral exploration. Economic Geology, 111, 1187-1222.

Mao, M., Rukhlov, A.S., Rowins, S.M., Hickin, A.S., Ferbey, T., Bustard, A., Spence, J., and Coogan, L.A., 2017. A novel approach using detrital apatite and till geochemistry to identify covered mineralization in the TREK area of the Nechako Plateau, British Columbia. In: Ferbey, T., Plouffe, A., and Hickin, A.S., (Eds.), Indicator Minerals in Till and Stream Sediments of the Canadian Cordillera. Geological Association of Canada Special Paper Volume 50, and Mineralogical Association of Canada Topics in Mineral Sciences Volume 47, pp. 191-243.

McDonough, M.R., Simony, P.S., Morrison, M.L., Oke, C., Sevigny, J.H., Robbins, D.B., Seigel, S.G., and Grasby, S.E., 1991. Howard Creek, British Columbia. Geological Survey of Canada Open File 2411, 1:50,000 scale.

McDonough, M.R., Simony, P.S., Sevigny, J.H., Robbins, D.B., Raeside, R., Doucet, P., Pell, J., and Dechesne, R.G., 1992. Geology of Nagle Creek and Blue River, British Columbia (83D/2 and 83D/3). Geological Survey of Canada Open File 2512, 1:50,000 scale.

Millonig, L.J., Gerdes, A., and Groat, L.A., 2012. U-Th-Pb geochronology of meta-carbonatites and meta-alkaline rocks in the southern Canadian Cordillera: A geodynamic perspective. Lithos, 152, 202-217.

Murphy, D.C., (compiler), 2007. Geology, Canoe River, British Columbia-Alberta. Geological Survey of Canada Map 2110A, 1:250,000 scale.

Ootes, L., Ferri, F., Milidragovic, D., and Wall, C., 2022. The age and provenance of the Lay Range assemblage provides an indirect record of basement to north-central Quesnellia, British Columbia. In: Geological Fieldwork 2021, British Columbia Ministry of Energy, Mines and Low Carbon Innovation, British Columbia Geological Survey Paper 2022-01, pp. 31-44.

Pell, J., 1994. Carbonatites, nepheline syenites, kimberlites and related rocks in B.C. British Columbia Ministry of Energy, Mines and Petroleum Resources, British Columbia Geological Survey Bulletin 88, 136 p.

Pell, J., and Simony, P.S., 1987. New correlations of Hadrynian strata, south-central British Columbia. Canadian Journal of Earth Sciences, 24, 302-313.

Raeside, R.P., and Simony, P.S., 1983. Stratigraphy and deformational history of the Scrip Nappe, Monashee Mountains, British Columbia. Canadian Journal of Earth Sciences, 20, 639-650.

Rudnick, R.L., and Gao, S., 2014. Composition of the continental crust. In: Holland, H.D., Turekian, K.K., and Rudnick, R.L., (Eds.), The Crust, Treatise on Geochemistry, 2nd Edition, Volume 4, Elsevier, Amsterdam, pp. 1-51. <http://dx.doi.org/10.1016/B978-0-08-095975-7.00301-6>

Rukhlov, A.S., Chudy, T.C., Arnold, H., and Miller, D., 2018. Field trip guidebook to the Upper Fir carbonatite-hosted Ta-Nb deposit, Blue River area, east-central British Columbia. British Columbia Ministry of Energy, Mines and Petroleum Resources, British Columbia Geological Survey GeoFile 2018-6, 67 p.

Rukhlov, A.S., Cui, Y., Cunningham, Q., Fortin, G., and Anderson, C., 2024. Geochemical signals of carbonatite-related critical metals in provincial stream sediments. In: Geological Fieldwork 2023, British Columbia Ministry of Energy, Mines and Low Carbon Innovation, British Columbia Geological Survey Paper 2024-01, pp. 97-122.

Rukhlov, A.S., Ootes, L., Creaser, R.A., Cunningham, Q.F., de Waal, F.S., and Wenger, D.K., 2025a. British Columbia carbonatites revisited: New whole rock Sr-Pb-Nd isotopic insights and drainage prospectivity trends. In: Geological Fieldwork 2024, British Columbia Ministry of Mining and Critical Minerals, British Columbia Geological Survey Paper 2025-01, pp. 119-139.

Rukhlov, A.S., Ootes, L., Creaser, R.A., Cunningham, F.Q., de Waal, S.F., and Wenger, D.K., 2025b. Supplementary data for British Columbia carbonatites revisited: New whole rock Sr-Pb-Nd isotopic insights and drainage prospectivity trends. British Columbia Ministry of Mining and Critical Minerals, British Columbia Geological Survey GeoFile 2025-09, 4 p.

Simandl, G.J., Mackay, D.A.R., Ma, X., Luck, P., Gravel, J., and Akam, C., 2017. The direct indicator mineral concept and QEMSCAN® applied to exploration for carbonatite and carbonatite-related ore deposits. In: Indicator Minerals in Till and Stream Sediments of the Canadian Cordillera, Ferbey, T., Plouffe, A. and Hickin, A.S., (Eds.), Geological Association of Canada, Special Paper Volume 50 and Mineralogical Association of Canada, Topics in Mineral Sciences Volume 47, pp. 175-190.

Simony, P.S., Ghent, E.D., Craw, D., and Mitchell, W., 1980. Structural and metamorphic evolution of the northeast flank of the Shuswap complex, southern Canoe River area, British Columbia. In: Crittenden, M.D., Coney, P.J., and Davis, G.H., (Eds.), Cordilleran Metamorphic Core Complexes. Geological Society of America, Memoir 153, pp. 445-461.

Warr, L.N., 2021. IMA-CNMNC approved mineral symbols. Mineralogical Magazine, 85, 291-320. <https://doi.org/10.1180/mgm.2021.43>

Wheeler, J.O., and Fox, P.E., 1964. Geology, Big Bend, Seymour Arm, east half, British Columbia. Geological Survey of Canada Preliminary Map, 12-1964, 1:253,440 scale.

Ya'acoby, A., 2014. The petrology and petrogenesis of the Ren carbonatite sill and fenites, southeastern British Columbia, Canada. Unpublished M.Sc. thesis, The University of British Columbia, Canada, 463 p.